Thickness Profile Estimation of Fluid-Carrying Non-Metallic Pipes

Maharshi B. Shah, Yuki Gao, Maryam Ravan, Reza K. Amineh
Applied Electromagnetics Research Lab, New York Institute of Technology, USA
{mshah41, ygao21, mravan, rkhalaja}@nyit.edu

***Abstract*—In oil, gas, transportation, and construction industries non-metallic pipes are rapidly replacing metallic pipes. Thus, it is crucial to have a reliable and robust nondestructive testing (NDT) technique to monitor the variation in the thickness profile of such pipes. Here, we propose a technique based on the near-field microwave holography and standardized minimum norm (SMN) to reconstruct the thickness profile of these pipes. We will also identify the fluid carried within the pipe which improves the thickness profile estimation process. The proposed methods are validated via simulation and experimental results.**

***Keywords*—microwave imaging, near-field holography, nondestructive testing.**

I. Introduction

Non-metallic pipes offer advantages such as: high strength, resilience to corrosion, light weight, low cost, and easy installation. These qualities make them highly attractive for various industries. Due to possible damages in these components, it is extremely crucial to develop a reliable nondestructive testing (NDT) technique for the thickness estimation of these pipes. Lack of such testing techniques can forge disastrous scenarios like leakage and bursting of the pipes. To address the above-mentioned requirement, microwave NDT has been considered as a promising inspection method [1], [2].

Two groups of microwave NDT techniques have been employed for inspection of non-metallic pipes, including: (1) imaging based on the raw responses [3], and (2) imaging based on more advanced processing such as synthetic aperture radar (SAR) processing (e.g., see [4], [5]), and near-field holography (e.g., see [6]-[9]). Particularly, in [9], near-field microwave holography has been proposed for inspection of double concentric non-metallic pipes. There, standardized minimum norm (SMN) approach has been employed to solve the relevant systems of equations to mitigate the depth biasing problem. To reduce the complexity and cost, narrowband frequency has been employed along with an array of receiver antennas.

Unlike the technique in [9] which provides qualitative images of double pipes, here, we propose a technique that allows for quantitative thickness estimation of a non-metallic pipe along with the identification of the fluid carried within the pipe. Identifying the carried fluid leads to lower errors in thickness estimation process. The proposed techniques will be validated via simulation and experimental results.

II. Theory

Fig. 1 illustrates the setup including a transmitter antenna to illuminate the pipe under test (PUT) and an array of N_A receiver antennas. The pipe has thickness of T_P and outer radius of R_{out}. The antennas scan a circular aperture, [0 to 2π] with radius of r_A at N_ϕ angles along the azimuthal direction ϕ. The scattered field, $E^{SC}(\phi)$, is measured at each sampling position, at N_ω frequencies within the band of ω_1 to ω_{N_ω}, by each receiver antenna. Such scattered response is then calibrated by subtracting the response of the pipe without defects from the response of the same pipe with defects. The image reconstruction process then provides images over N_r circles with radii $r_i = R_{out} - T_P + T_P(2i-1)/(2N_r)$, $i = 1,\ldots,N_r$ and $(R_{out}-T_P) < r_i < R_{out}$. Use of Born approximation in this technique leads to the linear property of the imaging system.

According to [9], the defect response, $E^{SC}_{a_m}(\phi,\omega_n)$, measured by the a_m-*th* receiver ($a_m = 1,\ldots,N_A$) over N_r circles can be written as:

$$E^{SC}_{a_m}(\phi,\omega_n) = \sum_{i=1}^{N_r} E^{SC,CD}_{i,a_m}(\phi,\omega_n) *_\phi f_i(\phi) \quad (1)$$

where $*_\phi$ denotes the convolution operator along ϕ axis, $f_i(\phi)$ denotes the defect's shape function on imaged circle $r = r_i$, and $E^{SC,CD}_{i,a_m}(\phi,\omega_n)$ denotes the collected point-spread function (PSF) on the *i*-th imaged circle. Similar to [9], PSFs are obtained *a priori* via measuring small defects called calibration defects (CDs) placed over imaged circles one at a time.

After applying discrete Fourier transforms (DFT) (with respect to ϕ) to both sides of (1), we obtain:

$$\tilde{E}^{SC}_{a_m}(k_\phi,\omega_n) = \sum_{i=1}^{N_r} \tilde{E}^{SC,CD}_{i,a_m}(k_\phi,\omega_n)\tilde{f}_i(k_\phi). \quad (2)$$

Writing (2) for all the frequencies and for all the receivers, a system of equations can be constructed at each Fourier variable k_ϕ as [9]:

$$\underline{\underline{\tilde{E}}}^{SC} = \underline{\underline{\tilde{D}}}\,\underline{\tilde{F}} \quad (3)$$

where

$$\underline{\underline{\tilde{E}}}^{SC} = \begin{bmatrix} \underline{\tilde{E}}^{SC}_1 \\ \vdots \\ \underline{\tilde{E}}^{SC}_{N_A} \end{bmatrix}, \underline{\underline{\tilde{D}}} = \begin{bmatrix} \underline{\tilde{D}}_1 \\ \vdots \\ \underline{\tilde{D}}_{N_A} \end{bmatrix}, \underline{\tilde{F}} = \begin{bmatrix} \tilde{f}_1(k_\phi) \\ \vdots \\ \tilde{f}_{N_r}(k_\phi) \end{bmatrix} \quad (4)$$

and

$$\underline{\tilde{E}}^{SC}_{a_m} = \begin{bmatrix} \tilde{E}^{SC}_{a_m}(k_\phi,\omega_1) \\ \vdots \\ \tilde{E}^{SC}_{a_m}(k_\phi,\omega_{N_\omega}) \end{bmatrix} \quad (5)$$

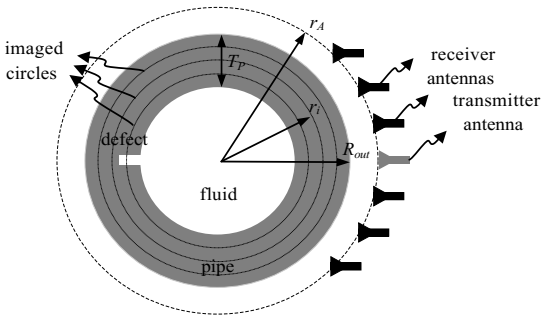

Fig. 1. Illustration of the cross section of the microwave measurement setup.

2022 IEEE/MTT-S International Microwave Symposium - IMS 2022 | 978-1-6654-9613-1/22/$31.00 ©2022 IEEE | DOI: 10.1109/IMS37962.2022.9865406

$$\underline{\underline{\tilde{\boldsymbol{D}}}}_{a_m} = \begin{bmatrix} \tilde{E}^{SC,CD}_{1,a_m}(k_\phi,\omega_1) & \cdots & \tilde{E}^{SC,CD}_{N_r,a_m}(k_\phi,\omega_1) \\ \vdots & \ddots & \vdots \\ \tilde{E}^{SC,CD}_{1,a_m}(k_\phi,\omega_{N_\omega}) & \cdots & \tilde{E}^{SC,CD}_{N_r,a_m}(k_\phi,\omega_{N_\omega}) \end{bmatrix}. \quad (6)$$

These systems of equations are solved using SMN approach at each k_ϕ to estimate the one-dimensional (1D) images in the Fourier domain, $\tilde{f}_i(k_\phi)$, $i = 1, \dots, N_r$. Then, inverse DFT is applied to reconstruct 1D images along ϕ. At the end, the normalized modulus of $f_i(n_\phi)$, $|f_i(n_\phi)|/M$, where M is the maximum of $|f_i(n_\phi)|$ for all r_i is plotted versus ϕ to obtain a 1D image of the defects on the *i*-th circle [9].

A. Pipe's Thickness Estimation

In [9], it is shown that excellent radial (range) resolution can be obtained due to the near-field nature of the imaging technique. Here, we exploit this characteristic to implement a quantitative evaluation of a single pipe's thickness. Rather than only providing the images, we proceed to provide an estimation of the thickness of the pipe at various angular positions. This helps to estimate the material loss due to the defects. For this purpose, we combine the 1D qualitative images $|f_i(n_\phi)|/M$, as below, to obtain a quantitative estimation of the thickness variation $T(n_\phi)$ as:

$$T(n_\phi) = T_P\left(1 - \frac{1}{N_r}\sum_{i=1}^{N_r}\frac{|\hat{f}_i(n_\phi)|}{M}\right). \quad (7)$$

In fact, this works by applying superposition of the effects of the defects on all the imaged circles. The effects due to larger defects along the radial direction will be observed on more imaged circles, in turn, leading to larger deviation from the nominal thickness when using (7).

In the results section, to evaluate the quality of the thickness estimations, we define the estimation error E_T as:

$$E_T = \sum_{i=1}^{N_r}\frac{\|T(n_\phi) - T_{true}(n_\phi)\|}{\|T_{true}(n_\phi)\|} \times 100 \quad (8)$$

where $T_{true}(n_\phi)$ is the true thickness profile for the pipe. The values of E_T will be shown on top of each relevant figure later.

B. Fluid Identification Approach

Identifying the type of fluid flowing through the pipe is crucial to reduce the thickness estimation error (using relevant collected PSFs in the processing). To estimate the fluid type, we propose an approach with the following steps:

1) Divide the responses acquired by all the N_A receivers into two sets: Set 1 responses for the odd numbered receivers and Set 2 responses for the even numbered receivers.
2) Guess N_f, number of possible fluids carried by the pipe and measure the PSFs related to these fluids *a priori*.
3) For each assumed fluid identified by number $n_f = 1 \dots, N_f$, we use Set 1 and Set 2 responses of the relevant PSFs and PUT scenarios and apply holographic algorithm on them separately to obtain the estimated thicknesses, $T_1^{n_f}(n_\phi)$ and $T_2^{n_f}(n_\phi)$, respectively.
4) For each assumed fluid in Step 3, the difference between the estimated thicknesses $T_1^{n_f}(n_\phi)$ and $T_2^{n_f}(n_\phi)$ is evaluated as:

$$\Delta T(n_f) = ||T_1^{n_f}(n_\phi) - T_2^{n_f}(n_\phi)|| \quad (9)$$

where $||\cdot||$ is the 2-norm operator.

5) The lowest ΔT identifies the true fluid carried by the pipe.

III. Simulation Results

Fig. 2 and Table 1 show the FEKO model and the respective parameter values used to study the performance of the proposed methods. The pipe has relative permittivity ε_r of 2.25 and loss tangent of 0.0004 and it carries a mixture of 20% water and 80% glycerin with electrical properties reported in [10].

To estimate the pipe's thickness profile, we employ an array of dipole antennas, which mechanically scans over a circular aperture [0 to 2π] in 181 grid points (every 2°) and measure the transmission *S*-parameters for each receiver antenna. Selection of dipole antennas is due to their large beamwidth leading to better cross-range resolutions in holographic imaging [11].

White Gaussian noise with signal-to-noise ratio (SNR) of 20 dB is added to the data. Then holographic imaging is applied to obtain 1D images over N_r = 4 circles with radii of $r_i = R_{out} - T_P + T_P(2i-1)/(2N_r)$, where $i = 1, \dots, N_r$. For this purpose, first, the PSFs corresponding to these four imaged circles are simulated by putting one small defect over that circle one at a time and simulate the responses. Then, the scattered responses (for PSFs and PUT) are obtained by subtracting the simulated responses without the presence of the defects from those with the presence of the defects. After reconstructing 1D images, the method in section II.A is employed to obtain the estimated thickness profile of the pipe as shown in Fig. 3. According to our study, the thickness estimation improves with the increase in the operation frequency. However, employing higher frequency increases the cost of data acquisition circuit.

To validate this approach, we assume the pipe could carry mixtures of water and glycerin with glycerin concentrations in the range of 55% to 100%. The mixture with glycerin concentration of 80% is used to obtain the PSFs. Then, 9 PUT models are simulated with various glycerin concentrations. Fig.

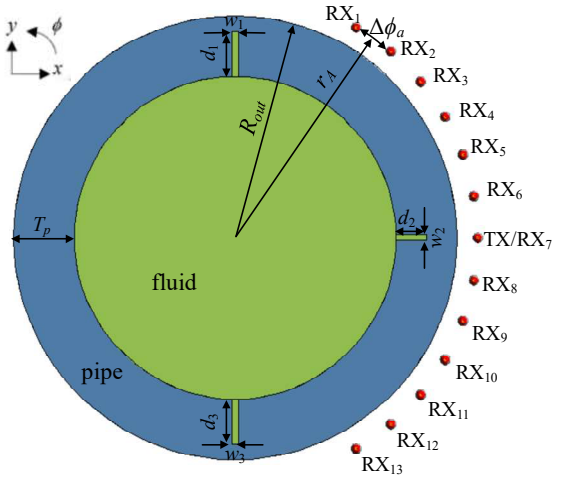

Fig. 2. Illustration of the FEKO simulation setup.

Table 1. Parameter values for the setup in Fig. 2.

N_A	$\Delta\phi_a$	r_A	R_{out}	T_P	ε_r	tanδ	f	fluid
13	10°	80 mm	73 mm	20 mm	2.25	0.0004	7 GHz	20% water and 80% glycerin

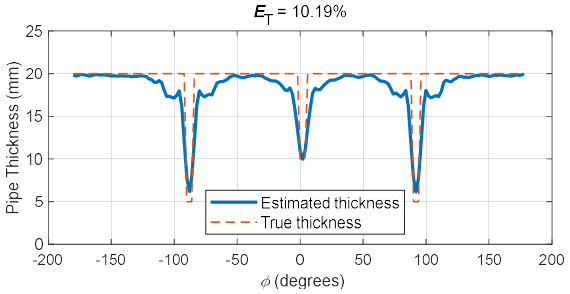

Fig. 3. Estimated thickness profile for the pipe shown in Fig. 2.

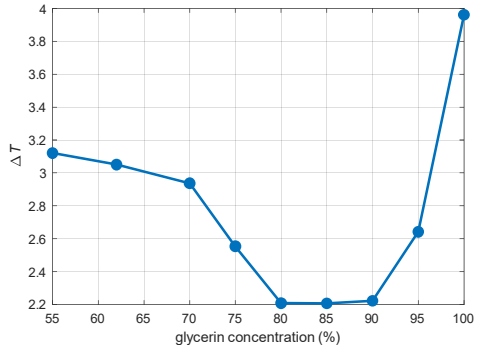

Fig. 4. Variation of ΔT in (9) when using data from two sets of receivers.

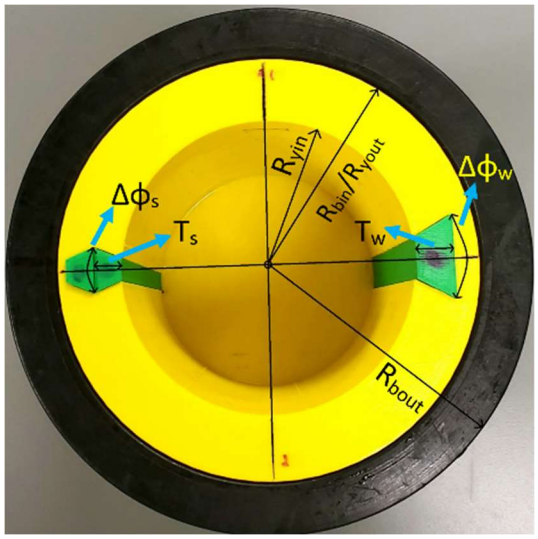

Fig. 5. Fabricated two-layer PUT including high density polyethylene (HDPE) layer seen in black, 3D printed layer seen in yellow, and 3D printed retractable pieces to create defects shown in green.

Table 2. Parameter values for the pipes and defects in Fig. 5.

R_{bout}	R_{bin}	R_{yout}	R_{yin}	$\Delta\phi_w$	T_w	$\Delta\phi_s$	T_s
82 mm	66 mm	66 mm	46 mm	25°	12 mm	15°	8 mm

4 shows that the computed ΔT values from (9) is minimum for the glycerin concentration of 80%. In other words, when the PUT and *a priori* measured PSFs have the same fluid type, the value of ΔT is minimum.

IV. Experimental Results

We use an array of 13, spatially distributed dipole antennas manufactured by TAOGLAS, similar to the simulation study. A two-layer pipe configuration is measured as shown in

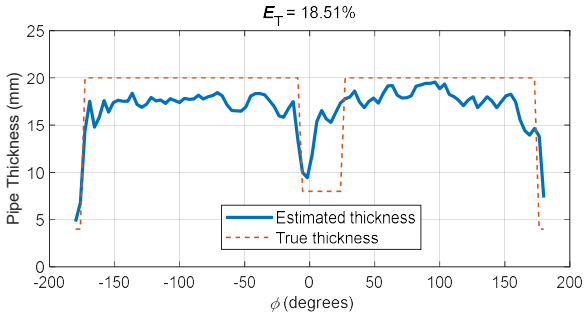

Fig. 6. Estimated thickness profile for the inner layer in Fig. 5.

Table 3. Variation of ΔT for different glycerin concentrations.

Glycerin concentration (%)	ΔT (%)
0	18.21
20	20.67
40	27.25

Fig. 5 with the values of the parameters shown in Table 2. Responses are collected at 10 frequencies over 5.5 GHz to 6.5 GHz. The antennas are measured by an Anritsu vector network analyzer (VNA) MS46122B via RF switching network. We use a circular scanning setup to collect responses at 100 positions covering 360° along ϕ. Fig. 6 shows the estimated thickness profile of the inner layer compared with the true thickness profile when the pipe is filled with 100% water.

Besides, Table 3 shows the variation of ΔT computed from (9) when using PSFs measured for 100% water but the test scenarios consists of glycerin concentratyions of 0%, 20% and 40%. It is observed that the smallest ΔT is obtained for 100% water (0% glycerin) confirming the validity of the fluid identification method.

V. Conclusion

We extended the qualitative near-field holographic imaging technique to implement quantitative thickness profile estimation of thick non-metallic pipes along the azimuthal direction. The theory and the results presented here can be easily extended to include the other cross-range direction, namely the longitudinal direction, as proposed in [9]. To achieve the best results when the pipe carries a fluid, we proposed an approach for fluid type identification as well. The performance of the proposed thickness estimation and fluid identification techniques were validated via simulation and experimental results. It is worth noting that the lower limit of the defect size that can be evaluated using the proposed technique is directly affected by the data acquisition circuitry's noise, ripples in the mechanical scanning, electromagnetic interferences, etc. An upper limit on the defect size is imposed due to the use of Born approximation.

Acknowledgment

This project has been supported by US national science foundation (NSF), award No. 1920098, and New York Institute of Technology's (NYIT) Institutional Support for Research and Creativity (ISRC) Grants.

REFERENCES

[1] A. Haryono, M. S. Rahman, and M. Abou-Khousa, "Inspection of non-metallic pipes using microwave non-destructive testing (NDT)," *IEEE Int. RF and Microw. Conf.*, 2018.

[2] M. S. Rahman, A. Haryono, Z. Akhter, and M. A. Abou-Khousa, "On the inspection of glass reinforced epoxy pipes using microwave NDT," *IEEE Int. Instr. Meas. Tech. Conf. (I2MTC)*, 2019.

[3] T. D. Carrigan, B. E. Forrest, H. N. Andem, K. Gui, L. Johnson, J. E. Hibbert, B. Lennox, and R. Sloan, "Nondestructive testing of nonmetallic pipelines using microwave reflectometry on an in-line inspection robot," *IEEE Trans. Inst. Meas.*, vol. 68, no. 2, pp. 586–594, Feb. 2019.

[4] M. T. Ghasr, K. Ying, and R. Zoughi, "3D millimeter wave imaging of vertical cracks and its application for the inspection of HDPE pipes," *AIP Conf. Proc.*, vol. 1581, no. 1, pp. 1531–1536, 2014.

[5] Laviada, J., B. Wu, M.T. Ghasr, and Reza Zoughi, "Nondestructive evaluation of microwave-penetrable pipes by synthetic aperture imaging enhanced by full-wave field propagation model," *IEEE Trans. on Instrum. and Meas.*, vol. 68, no. 4, pp. 1112–1119, Apr. 2019.

[6] Y. Gao, M. Ravan, and R. K. Amineh, "Fast, robust, and low-cost microwave imaging of multiple non-metallic pipes," *Electronics,* vol. 10, no. 15, 2021.

[7] H. Wu, M. Ravan, and R. K. Amineh, "Holographic near-field microwave imaging with antenna arrays in a cylindrical setup," *IEEE Trans. Microw. Theory & Tech.*, vol. 69, no. 1, pp. 418-430, 2021.

[8] R. K. Amineh, M. Ravan, and R. Sharma, "Nondestructive testing of nonmetallic pipes using wideband microwave measurements," *IEEE Trans. Microw. Theory & Tech.*, vol. 65, no. 5, pp. 1763-1772, May 2020.

[9] H. Wu, M. Ravan, R. Sharma, J. Patel, and R. K. Amineh, "Microwave holographic imaging of non-metallic concentric pipes," *IEEE Trans. Inst. & Meas.*, vol. 69, no. 10, pp. 7594–7605, Oct. 2020.

[10] P. M. Meaney, C. J. Fox, S. D. Geimer, and K. D. Paulsen, "Electrical characterization of glycerin: water mixtures: Implications for use as a coupling medium in microwave tomography," *IEEE Trans. Microw. Theory & Tech.*, vol. 65, no. 5, pp. 1471–1478, May 2017.

[11] D. M. Sheen, D. L. McMakin, and T. E. Hall, "Three-dimensional millimeter-wave imaging for concealed weapon detection," *IEEE Transactions on Microwave Theory and Techniques*, vol. 49, no. 9, pp. 1581–1592, 2001.